

A. L. LONDON

Professor.
Mem. ASME

G. KLOPFER

Graduate Student.

Mechanical Engineering Department,
Stanford University,
Stanford, Calif.

S. WOLF

Engineer, General Electric
Atomic Power Equipment Department,
San Jose, Calif.

Oblique Flow Headers for Heat Exchangers

The problem of the design of oblique flow headers for heat exchangers flowing low density fluids is considered. It is demonstrated by test that the theory already available in the literature provides an adequate basis for design for the single-pass "parallel flow" and "counterflow" configurations. The theory is summarized in the form of design equations and illustrated by specific application to the air-side flow in a gas turbine regenerator.

Introduction

IN energy conversion systems involving gas flow heat exchangers, the header configurations have a definitive influence on system envelope geometry. The regenerative cycle gas turbine engine is an extreme example of such a system. The highly compact surfaces employed tend to result in cores of large frontal area and short flow length. The sketch, Fig. 1, illustrates a folded core concept used to reduce the header volume. However, if the pressure drop across the core is not uniform the flow distribution over the transfer surfaces will not be uniform and a serious reduction in heat exchanger performance may be the penalty.

From this viewpoint, the design objective for the header is to provide for acceptably uniform flow with acceptable system geometry and flow stream mechanical energy losses. In effect, uniformity of flow distribution is the dominating function of the headers.

Wilson [1]¹ describes a design method where the inflow to the header is roughly normal to the heat transfer core face. In con-

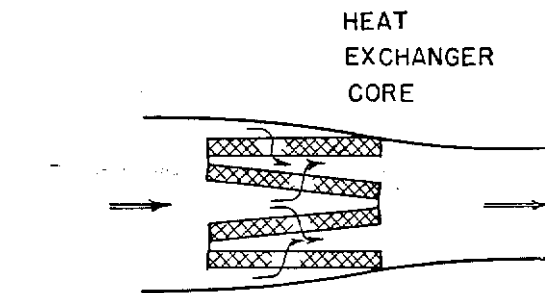


Fig. 1 Folded core heat exchanger illustrating an oblique flow header configuration

trast, this presentation is concerned with headers where the inflow is parallel to the heat transfer core face. The configurations considered specifically are described in Fig. 2.

This presentation is a condensation of the theoretical and experimental results reported in [2, 3]. The theory treats with three of the four configurations in Fig. 2, namely, the parallel flow, counterflow, and free discharge geometries. The experimental work was largely confined to the parallel and counterflow configurations; however, some limited testing was done with the two-pass parallel flow configuration in Fig. 2, with the view to investigate the validity of applying the single-pass theory to the two-pass situation. One of the idealizations of the theory

Nomenclature

A = flow area, sq ft
 g_c = proportionality factor in Newton's Second Law = 32.2 (lb/#)(ft/sec²)
 G = flow mass velocity = velocity $\times \rho$, lb/hr sq ft
 h = velocity head = $\rho u_{ave}^2 / 2g_c$, #/sq ft, in. of water
KE = flow stream kinetic energy rate ft #/sec
 l = flow length through matrix, ft
 L = long dimension of header, ft
 N_R = Reynolds number, dimensionless
 p = matrix porosity, flow void space/matrix volume, dimensionless
 P = fluid pressure, #/sq ft, in. of water
 ΔP = pressure drop, #/sq ft, psi, in. of water (see equation (1) for ΔP_i)

r_h = hydraulic radius for flow through the matrix, ft
 t = the x -coordinate along the matrix face in Fig. 19
 u = the fluid velocity component in the x -direction, fps
 v = the fluid velocity component in the y -direction, fps
 w = the fluid velocity along a streamline, fps
 x = Cartesian coordinate defined in Fig. 4, ft
 X = x/L
 y = Cartesian coordinate defined in Fig. 4, ft
 Y = y_{wall}/y_0
 z = Cartesian coordinate defined in Fig. 4, ft
 Z = z_{wall}/y_0

α = matrix friction area per unit volume, ft sq/cu ft
 δ = on velocity means deviation from average
 Δ = on pressure means pressure drop
 ϵ = effectiveness
 ρ = fluid density, pcf
 ω = airflow rate, lb/sec, lb/hr

Subscripts

i , denotes inlet of inlet header
 m , denotes matrix
 0 , denotes outlet of exit header
 t , denotes "total" in distinction to static pressure, $P_t = P + \frac{1}{2} \rho u^2$
ave, denotes average
Miscellaneous
lb, denotes pound mass in distinction to #
#, denotes pound force in distinction to lb

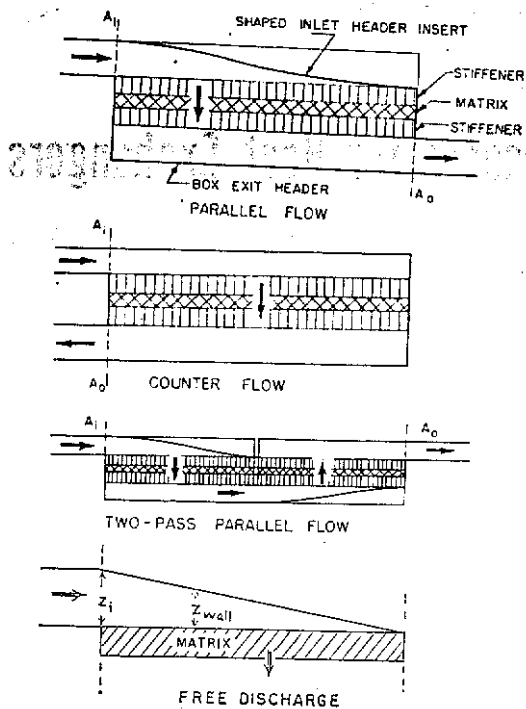


Fig. 2 The four types of oblique flow headers. Experimental results obtained only for the single-pass parallel flow and counterflow configurations, and for the two-pass parallel flow configuration.

is that the velocity profile is uniform at the inlet of the inlet header. Skewed velocity profiles, such as described in Fig. 3, were investigated experimentally to determine if the theory predictions were reasonably valid for actual design situations where the inlet profile is generally not uniform.

The theoretical methodology is largely based on the work of Perlmutter and Heyda [4, 5]. The mathematical model for the exit header analysis differs for these two authors and the Heyda model is selected for the present treatment as it is well substantiated experimentally. The analysis of header losses into inlet and exit components and the allowance for different fluid densities for the inlet and exit headers represent a simple, new contribution to the theory. It is believed that these extensions and the summary of results into convenient equations will be of value to the heat exchanger designer.

The specific purposes of this presentation are to:

- 1 Summarize the analytical results, including a detailed analysis of losses, for the three single-pass configurations—parallel flow, counterflow, and free discharge.
- 2 Present test results for the single-pass parallel flow and counterflow configurations and for the two-pass parallel flow configuration, both for “theory-shaped” headers and for other shapes not conforming to the theory. These results are for a fairly uniform, turbulent-type velocity distribution at the inlet, Fig. 3(d).
- 3 Present test results and limited theory results for the influence of nonuniform velocity profiles at the header inlet. These results are for the single-pass parallel flow and counterflow configurations.
- 4 Illustrate the application of the results to the design of practical oblique flow headers for heat exchangers.

Theory Results

The mathematical models analyzed for the parallel flow, counterflow, and free discharge configurations are described in Fig. 4. The applicable idealizations follow:

- 1 Inlet and exit header densities are separately constant.
- 2 Inlet header velocity, u_i , is uniform at $x = 0$.

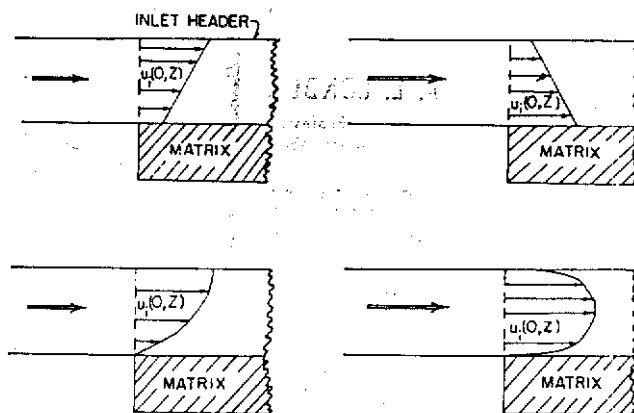


Fig. 3 Inlet velocity profiles: (a) favorable skew, linear; (b) unfavorable skew, linear; (c) favorable skew, sine; (d) typical turbulent profile characteristic of the first series of tests

- 3 The flow velocity in the inlet header is a function of x only.
- 4 The inlet header pressure is a function of x only.
- 5 The exit header pressure is a function of x only, but the velocity has a two-dimensional variation.
- 6 The inlet and exit header flows are loss-free (inviscid).

The conditions imposed on the system are:

- 1 The exit header has a box shape

$$Y(X) = 1 \text{ or } y_{\text{wall}}/y_0 = 1.$$

- 2 The mass flow distribution through the matrix is uniform; i.e., $v_m = \text{const}$ flowing into the exit header.
- 3 In order to provide for 2 it is necessary to shape the inlet header so that the inlet pressure profile $P(x)$ matches the exit pressure profile to make ΔP_{matrix} constant with x (see Fig. 4).

The important results of the analysis are:

- 1 $P(x)$ for the headers.
- 2 $u_o(y)$ for the velocity at the exit of the exit header.
- 3 Required shape of the inlet header $Z(x)$.
- 4 $u(x)$ for the velocity in the inlet header.
- 5 Loss components chargeable to the inlet and exit headers.

The details of the derivations are presented in the Appendix.

It is evident from the foregoing that the treatment is one-dimensionalized with respect to pressure in both headers and also velocity in the inlet header, but the outlet header velocity $u(x, y)$ is two-dimensional. As will be shown, the one-dimensional idealization for pressure is justified by experiment. The justification for selecting a box shape of the exit header is that it yields a minimum pressure drop [4, 5].

Even though the flow in each of the headers is loss-free, according to idealization (6), there is a header loss chargeable to the inlet and exit header and matrix system. This loss has two sources: (a) The kinetic energy dissipation as the flow leaves the inlet header at a fairly high velocity and collides with the matrix, and (b) the kinetic energy “excess” in the exit header associated with the nonuniform velocity profile $u_o(y)$ shown in Fig. 4(a, b). The header loss is defined as the loss in the total pressure that is not chargeable to the matrix; namely,

$$\frac{\Delta P_i}{h_i} = \frac{(P_{i,t} - P_{o,t}) - \Delta P_{\text{matrix}}}{h_i} \quad (1)$$

As the dynamic head h_o in the exit total pressure $P_{o,t}$ is based on a bulk average $u_{o,\text{ave}}$, any nonuniformity in u_o will appear as a “bookkeeping” loss in kinetic energy.

The experimental evidence supporting these idealizations will be presented later.

The important analytical results for the single-pass parallel flow header configuration, Fig. 4(a), follow:

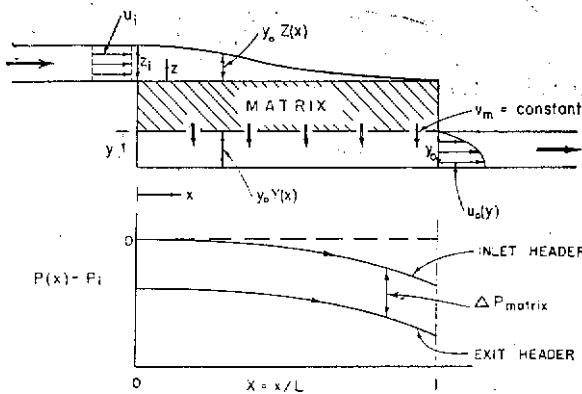


Fig. 4(a) Parallel flow

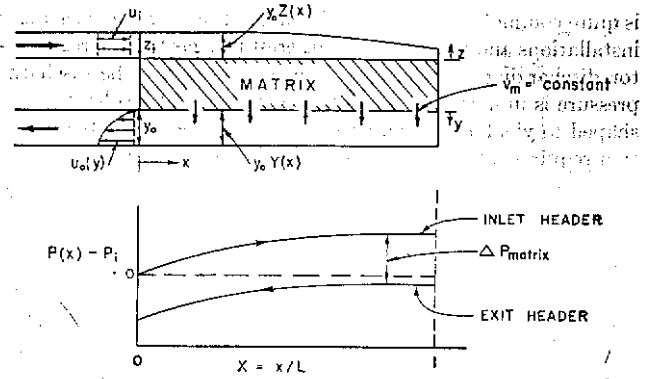


Fig. 4(b) Counterflow

Exit Header. Box configuration $Y(X) = 1$ (imposed condition (1)).

$$\text{Pressure, } \frac{P_i - P(X)}{h_0} = \frac{\Delta P_{\text{matrix}}}{h_0} + \frac{\pi^2 X^2}{4} \quad (2)$$

$$\text{Velocity, } \frac{u_0}{u_{0,\text{ave}}} = \frac{\pi}{2} \sin\left(\frac{\pi y}{2 y_0}\right) \quad (3a)$$

$$\frac{(u_0^3)_{\text{ave}}}{(u_{0,\text{ave}})^3} = \frac{\pi^2}{6} = 1.645 \quad (3b)$$

Inlet Header

$$\text{Pressure, } \frac{P_i - P(X)}{h_i} = \frac{\pi^2}{4} X^2 \frac{\rho_i}{\rho_0} \left(\frac{z_i}{y_0}\right)^2 \quad (4)$$

$$\text{Geometry, } Z = \frac{(1 - X)}{\left[\left(\frac{\rho_i}{\rho_0}\right) \left(\frac{\pi^2}{4}\right) X^2 + \left(\frac{y_0}{z_i}\right)^2\right]^{1/2}} \quad (5)$$

$$\text{Velocity, } \frac{u}{u_i} = \sqrt{\frac{\rho_i}{\rho_0} \left(\frac{z_i^2}{y_0^2}\right) \frac{\pi^2}{4} X^2 + 1} \quad (6a)$$

$$\frac{(u^2)_{\text{ave}}}{u_i^2} = 1 + \frac{\pi^2}{12} \frac{\rho_i}{\rho_0} \left(\frac{z_i}{y_0}\right)^2 = 1 + 0.822 \frac{\rho_i}{\rho_0} \left(\frac{z_i}{y_0}\right)^2 \quad (6b)$$

Note that from continuity

$$\frac{h_0}{h_i} = \frac{\rho_i}{\rho_0} \left(\frac{z_i}{y_0}\right)^2 \quad (6c)$$

The mathematical model for the counterflow header configuration is described in Fig. 4(b). In contrast to the parallel flow configuration, the inlet header functions as a diffuser to decelerate the flow. The outlet header behaves exactly like that for the parallel flow configuration with a flow acceleration and a drop in pressure in the flow direction.

The important analytical results for the single-pass counterflow configuration follow:

Exit Header. Box configuration $Y(X) = 1$ (imposed condition (1)).

$$\text{Pressure, } \frac{P_i - P(X)}{h_0} = \frac{\Delta P_{\text{matrix}}}{h_0} - \frac{\pi^2}{4} [1 - (1 - X)^2] \quad (7)$$

$$\text{Velocity, } \frac{u_0}{u_{0,\text{ave}}} = \frac{\pi}{2} \sin\left(\frac{\pi y}{2 y_0}\right) \quad (8a)$$

$$\frac{(u_0^3)_{\text{ave}}}{(u_{0,\text{ave}})^3} = \frac{\pi^2}{6} = 1.645 \quad (8b)$$

Inlet Header

$$\text{Pressure, } \frac{P(X) - P_i}{h_i} = \frac{\rho_i}{\rho_0} \left(\frac{z_i}{y_0}\right)^2 \frac{\pi^2}{4} [1 - (1 - X)^2] \quad (9)$$

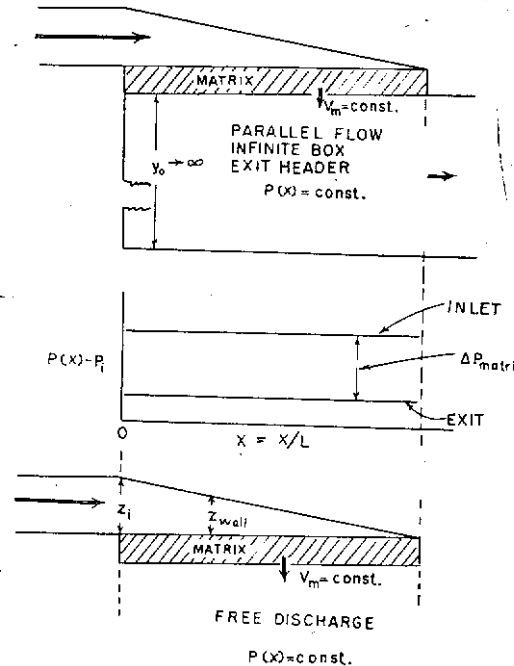


Fig. 4(c) Free discharge, as a limiting case of parallel flow

Fig. 4 Mathematical models for the theoretical analysis

$$\text{Geometry, } Z = \frac{2}{\pi} \sqrt{\frac{\rho_0}{\rho_i}} = 0.636 \sqrt{\frac{\rho_0}{\rho_i}} \quad (10)$$

(A box header is required for a minimum inlet header loss.)

$$\text{Velocity, } \frac{u}{u_i} = (1 - X) \quad (11a)$$

$$\frac{(u^2)_{\text{ave}}}{u_i^2} = \frac{1}{3} \quad (11b)$$

Note that from equation (10) and continuity

$$\frac{h_0}{h_i} = \frac{\rho_i}{\rho_0} \left(\frac{z_i}{y_0}\right)^2 = \frac{4}{\pi^2} = 0.405 \quad (11c)$$

In contrast to the parallel flow configuration, where the inlet header dimension z_i can be either larger or smaller than the outlet dimension y_0 , for counterflow z_i must be $0.636 y_0 \sqrt{(\rho_0/\rho_i)}$ in order to assure the matching pressure profile needed for uniform flow distribution and for a minimum header loss. This point is established in the derivations presented in the Appendix.

The free discharge header configuration is a special case of the parallel flow configuration with the exit header dimension y_0 going to infinity, as indicated in Fig. 4(c). This header configuration

is quite commonly encountered in air-conditioning heat exchanger installations and may also be of interest in a gas turbine regenerator, discharging straight into an exhaust stack. The discharge pressure is uniform for this situation so the inlet header must be shaped to yield a uniform pressure. This pressure match condition requires a triangular shape, with uniform velocity

$$\text{Geometry, } Z = (1 - X) \quad (12)$$

$$\text{Velocity, } \frac{u}{u_i} = 1 \quad (13a)$$

$$\frac{(u^2)_{\text{ave}}}{u_i^2} = 1 \quad (13b)$$

In the following consideration the overall loss of flow stream mechanical energy, equation (1), will be analyzed in terms of its two components: (a) The kinetic energy dissipation as the flow leaves the inlet header, and (b) the kinetic energy "excess" associated with the nonuniform velocity profile $u_0(y)$, shown in Fig. 4, which is chargeable to the exit header.

For the *parallel flow* configuration from equations (2) and (6c), equation (1) becomes

$$\begin{aligned} \frac{\Delta P_t}{h_i} &= \left(\frac{h_0}{h_i}\right) \left[\frac{\pi^2}{4} + \frac{h_i}{h_0} - 1\right] = 1.467 \frac{\rho_i}{\rho_0} \left(\frac{z_i}{y_0}\right)^2 + 1 \\ &= 1.467 \frac{h_0}{h_i} + 1 \quad (14) \end{aligned}$$

For the *counterflow* configuration, from equations (7) and (11c), equation (1) becomes

$$\frac{\Delta P_t}{h_i} = 1 - \frac{h_0}{h_i} = 1 - \frac{4}{\pi^2} = 0.595 \quad (15)$$

Two interesting design conclusions are immediately evident; namely, (a) the optimum counterflow configuration has the much smaller loss, and (b) unlike the parallel flow situation, the counterflow loss does not depend on inlet to outlet flow stream density ratio. A typical parallel flow design would be with

$$\left(\frac{z_i}{y_0}\right)^2 = \frac{\rho_0}{\rho_i} \quad \text{or } h_0 = h_i$$

so that $\Delta P_t/h_i = 2.467$, 4.15 times the comparable counterflow loss.

For the *free discharge* configuration the exit header loss is nil. $P_{0,t} \approx P_0$, $P_{i,t} = P_i + h_i$.

$$\Delta P_{\text{matrix}} = (P_i - P_0)$$

and equation (1) becomes

$$\frac{\Delta P_t}{h_i} = 1 \quad (16)$$

In comparison with equations (14) and (15), it is seen that the header loss for the oblique flow inlet, free discharge configuration is intermediate to the parallel flow and counterflow configurations.

It is of interest to analyze the total header loss into components chargeable to the inlet and the exit headers, respectively.

For the inlet header, the loss is postulated to be all the kinetic energy leaving the header and entering the matrix where it is dissipated, with no pressure rise, and appears as an increase of enthalpy of the flow.

$$\frac{\text{KE}_{\text{inlet}}}{\omega} = \frac{1}{\rho_i L v_m} \int_0^L \rho_i v_m \frac{u^2}{2g_c} dx \quad (17)$$

But $v_m = \text{const}$ with x and so is ρ_i ; thus the inlet loss becomes

$$\frac{\text{Inlet loss}}{h_i} = \frac{(u^2)_{\text{ave}}}{u_i^2} \quad (17a)$$

By equations (6b) and (6c) for the inlet header of the *parallel flow* configuration

$$\frac{\text{Inlet loss}}{h_i} = 1 + \frac{\pi^2}{12} \left(\frac{h_0}{h_i}\right) \quad (17b)$$

By equation (11b) for the inlet header of the *counterflow* configuration

$$\frac{\text{Inlet loss}}{h_i} = \frac{1}{3} \quad (17c)$$

By equation (13b) for the inlet header of the *free discharge* configuration

$$\frac{\text{Inlet loss}}{h_i} = 1 \quad (17d)$$

For the exit header for both the counterflow and parallel flow configurations the loss is the kinetic energy "excess" associated with the nonuniform velocity profile $u_0(y)$ at the exit section. This quantity is in excess over h_0 which is based on a bulk average velocity by convention. So, essentially, this is a bookkeeping rather than a real loss. The kinetic energy associated with the nonuniform velocity profile $u_0(y)$ at the outlet header exit is

$$\frac{\text{KE}_0}{\omega} = \frac{1}{y_0 \rho_0 u_{0,\text{ave}}} \int_0^{y_0} (\rho_0 u_0) \frac{u_0^2}{2g_c} dy = \frac{1}{(u_{0,\text{ave}})} \frac{(u_0^2)_{\text{ave}}}{2g_c}$$

The excess kinetic energy head above the nominal magnitude evaluated using a bulk average velocity is

$$\begin{aligned} \frac{\text{Exit loss}}{h_0} &= \frac{\rho_0 \text{ excess KE}_0/\omega}{h_0} = \frac{(u_0^2)_{\text{ave}}}{(u_{0,\text{ave}})^2} - 1 \\ &= \frac{\pi^2}{6} - 1 = 0.645 \quad (18) \end{aligned}$$

where the numerical result comes from equation (3b).

Adding the appropriate components will yield the total header losses previously derived in equations (14-16). For instance, for the parallel flow configuration from equations (17b) and (18)

$$\frac{\Delta P_t}{h_i} = 1 + \frac{\pi^2}{12} \left(\frac{h_0}{h_i}\right) + \left(\frac{\pi^2}{6} - 1\right) \frac{h_0}{h_i} = \frac{h_0}{h_i} \left[\frac{\pi^2}{4} + \frac{h_i}{h_0} - 1\right]$$

which is the same as equation (14).

In summary, the postulated "loss-free" flow theory for the headers provides expressions for the losses to be charged to the headers in the header-matrix complex. Equations (14-16) provide the total header losses and equations (17b, c, d) provide the inlet header contribution, while equation (18) provides the exit header contribution.

One of the idealizations of the foregoing theory is that the inlet header velocity u_i is uniform at $x = 0$, Fig. 4. The following consideration is for the effect of a nonuniform or skewed inlet velocity profile, such as described in Fig. 3. The results are quite approximate because of the simplifications made in the analysis; they will, however, provide a basis for rationalizing the test results.

In the previous treatment for the inlet header loss, two sources were noted, namely:

1 The kinetic energy of the fluid leaving the inlet header and dissipating in the matrix.

2 A bookkeeping loss due to the nonuniform exit velocity producing an excess kinetic energy over that credited to the header which is calculated for a bulk average velocity.

For a skewed inlet profile, a third component must be included, namely:

3 A "bookkeeping" gain associated with the "excess" kinetic energy at the inlet of the inlet header due to the nonuniform $u_i(z)$.

The loss chargeable to the inlet header is the difference between that part of the kinetic energy leaving the inlet header which is dissipated upon impact with the matrix and the excess kinetic energy, due to flow nonuniformity, entering the inlet header, namely,

$$\left(\frac{\text{Inlet loss}}{h_i} \right)_{\text{chargeable}} = \left(\frac{\text{KE}/\omega}{h_i/\rho_i} \right)_{\text{dissipated}} - \left(\frac{\text{KE}/\omega}{h_i/\rho_i} \right)_{\text{excess entering}} \quad (19)$$

The chargeable loss is less than the actual loss due to the book-keeping gain of the excess kinetic energy at the inlet and not included in $P_{i,e}$.

The actual loss of the flow leaving the inlet header is that part of the kinetic energy leaving the inlet header and entering the matrix which is dissipated, with no pressure rise, and appears as an increase of the enthalpy of the flow

$$\left(\frac{\text{KE}/\omega}{h_i/\rho_i} \right)_{\text{dissipated}} = \left(\frac{\text{KE}/\omega}{h_i/\rho_i} \right)_{\text{leaving inlet header}} - \frac{\rho_i v_m^2}{2g_c h_i} \quad (20)$$

The matrix dynamic head term, the last term in equation (20), is generally negligibly small for A_i/A_m ratios less than 1/5.

The kinetic energy leaving the inlet header (entering the matrix) may be considered to consist of three parts:

(a) h_i = the nominal kinetic energy entering the inlet header.

(b) $\rho_i \text{KE}/\omega_{\text{excess entering}}$ = the excess over nominal kinetic energy entering the inlet header.

(c) $\rho_i \text{KE}/\omega_{\text{produced}}$ = the reversible header flow production of kinetic energy due to the inlet header pressure profile $P(X)$.

This production of kinetic energy is positive for the parallel flow header, which acts as a nozzle, and negative for the counterflow header, which acts as a diffuser. A uniform v_m is one of the important conditions previously imposed on the header heat exchanger system; and as before, inviscid or loss-free flow is specified as an idealization. As a result, the production of kinetic energy term depends only on $P(X)$, irrespective of the inlet velocity profile. The actual loss is then

$$\left(\frac{\text{KE}/\omega}{h_i/\rho_i} \right)_{\text{dissipated}} = \left(\frac{\text{KE}/\omega}{h_i/\rho_i} \right)_{\text{produced}} + \left(\frac{\text{KE}/\omega}{h_i/\rho_i} \right)_{\text{excess entering}} + \frac{h_i}{h_i} - \frac{\rho_i v_m^2}{2g_c h_i} \quad (21)$$

The term for the matrix dynamic head, $\frac{\rho_i v_m^2}{2g_c h_i}$, may be neglected compared to h_i/h_i (approximately 1 percent error since $A_i/A_m = 1/8$ for the parallel flow test header and $A_i/A_m = 1/12$ for the counterflow test header).

The loss chargeable to the inlet header, equation (19), is the actual loss minus the excess kinetic energy at the inlet, because only the nominal kinetic energy is credited to the $P_{i,e}$. Thus the chargeable inlet header loss is

$$\left(\frac{\text{Inlet loss}}{h_i} \right)_{\text{chargeable}} = \left(\frac{\text{KE}/\omega}{h_i/\rho_i} \right)_{\text{produced}} + 1 \quad (22)$$

As the kinetic energy produced is independent of the inlet velocity profile, depending only on $P(X)$, it is to be expected that the loss chargeable to the inlet header will be independent of the inlet velocity profiles. Moreover, if one accepts the approximation that $P(X)$ in the inlet header with a skewed inlet profile is essentially that for the same theory shape header with the uniform profile, it follows that the previously developed expressions, equations (17b, c, d) will also apply. That is, inlet profile shape does not have a strong influence on total¹ header loss as defined in equation (1). This conclusion, in view of the approximations introduced in the development, requires some experimental input to determine the degree of nonuniformity that can be tolerated in the inlet profile shape. Obviously very strong nonuni-

¹ If the matrix flow distribution is uniform, $v_m = \text{const}$, the inlet header contribution to the total loss will not be influenced by the inlet profile and equation (18) is applicable.

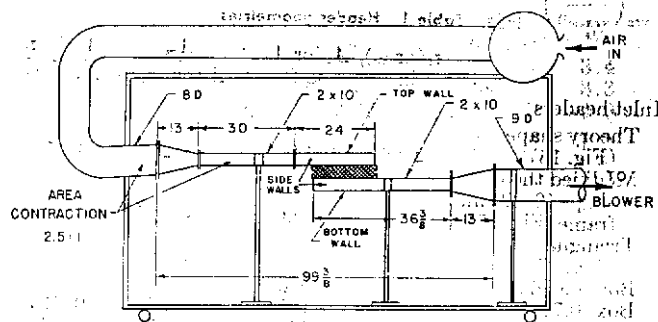


Fig. 5 Test system flow diagram, dimensions in in. Single-pass parallel flow configuration shown.

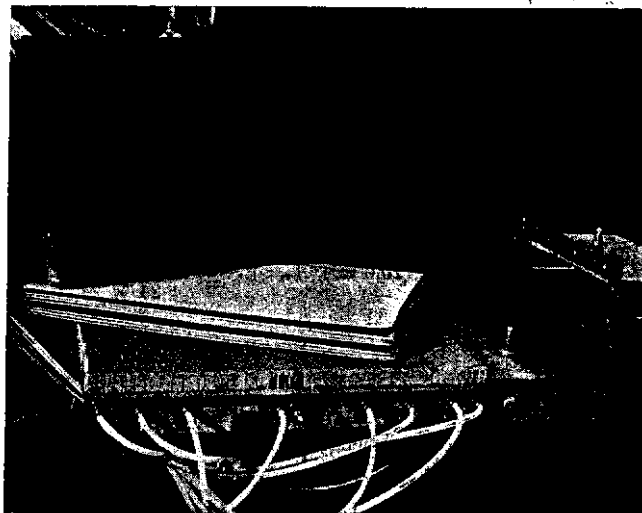


Fig. 6 Screen matrix and HEXCEL stiffeners

formities $u_i(z)$ will significantly influence $P(X)$ and the uniformity of the matrix flow v_m .

Experimental Results

After a brief description of the test system, data will be presented supporting the idealizations made in the analysis. A flow nonuniformity criterion will be developed and the actual header performance will be presented in terms of pressure profile, header total head loss, and flow nonuniformity. Theory-shaped headers will be considered and also designs that differ from the theory. The performance of a two-pass parallel flow configuration will also be presented to indicate the type of extrapolation one may make of the single-pass theory. The foregoing results are all for a turbulent-type velocity profile, Fig. 3(d), at the inlet of the inlet header. After this presentation, the results for various skewed inlet velocity profiles such as in Figs. 3(a, b, c) are presented.

Test System

The flow system for the single-pass parallel flow configuration is shown schematically in Fig. 5. The matrix arrangement consisting of two HEXCEL stiffeners and seven pads of five screens each is shown in Fig. 6. The stiffeners proved to be very effective in eliminating header-shape distortions due to the screens bulging and sagging. Wooden inserts introduced into the box-shaped sheet metal header provided the test shapes for the inlet header.

Eight header sets were tested. Four of these are single-pass parallel flow configurations, three are counterflow, and one is a two-pass parallel flow configuration, Fig. 2. Table 1 provides the important dimensions for the headers, and Table 2 provides the matrix information. More details on the test system are available in [2, 3, 7].

Table 1 Header geometries

	z_i (or y_0), in.	A_i (or A_0), sq ft	$\frac{A_m}{A_i}$ (or A_0)	$\frac{A_i}{A_0} = \frac{z_i}{y_0}$
Inlet headers				
Theory shape (Fig. 16)	2.06	0.143	8.25	0.97
Modified theory shape (0.020-in. frame, Fig. 17)	2.08	0.144	8.17	0.98
Triangular (Fig. 17)	2.06	0.143	8.25	0.97
Box (0.636 ratio)	1.35	0.0938	12.60	0.636
Box (0.713 ratio)	1.51	0.105	11.25	0.713
Box (0.97 ratio)	2.06	0.143	8.25	0.97
Exit headers				
Box for parallel flow, counter-flow, and second pass of 2-pass parallel flow	(2.12)	(0.147)	(8.00)	
Box for first pass of 2-pass parallel flow	(2.10)	(0.146)	(8.10)	

Table 2 Matrix geometry

Number of screen layers	35
Frontal area (17.0 in. \times 10.0 in.), A_m sq ft	1.18
Mesh designation per in.	24 \times 24.5
Wire diameter, in.	0.0135
Estimated porosity, p	0.725
area density, α sq ft/cu ft	980
hydraulic radius, r_h ft	0.740×10^{-3}
flow length, l ft	0.0787
l/r_h	106.5
Stiffeners (HEXCEL) Flow length, in.	2×1.00
cell size, in.	1/8
wall, in.	0.002

Experimental Verification of Idealizations

For the box exit header, one verification of the idealizations leading to the analytical results, equations (2), (3a, b) and (7), (8a, b), is provided by a comparison of the measured exit velocity profile with the theory prediction, equations (3a), (8a). This is done in Fig. 7 and the agreement is excellent.

The validity of the idealization of pressure as a function of x only, in both the inlet and exit headers, is provided by a comparison of the narrow side-wall pressure tap readings with those of the bottom and top walls. The side-wall taps are located at a plane about one fourth of the side-wall dimension from the matrix stiffener face for both the inlet and outlet headers. These comparisons are presented in Fig. 8 by the different types of data points for the experimental pressure profile. The close agreement of the two sets of pressure readings strongly supports the one-dimensional idealization for the pressure.

Flow Uniformity Criterion

Before presenting the header performance, it is necessary to specify a criterion that is descriptive of flow nonuniformity through the matrix. It is necessary that this criterion be readily evaluated from test results and be usable by the designer to estimate the heat transfer performance penalty due to the nonuniformity. Fig. 8 presents a typical set of pressure data. After the pressure profiles are plotted, the $\Delta P_{matrix}/h_i$ is read from the graph at 11 equally spaced abscissa values over the range $0 \leq X \leq 1$. The $\sqrt{\Delta P_{matrix}/h_i}$ is then calculated and $v_m/v_{m,ave}$ is formed as

$$\frac{v_m}{v_{m,ave}} = \frac{\sqrt{\Delta P_{matrix}/h_i}}{\sqrt{\Delta P_{matrix}/h_i}_{ave}}$$

The 11 ordinate trapezoid rule is used to form the

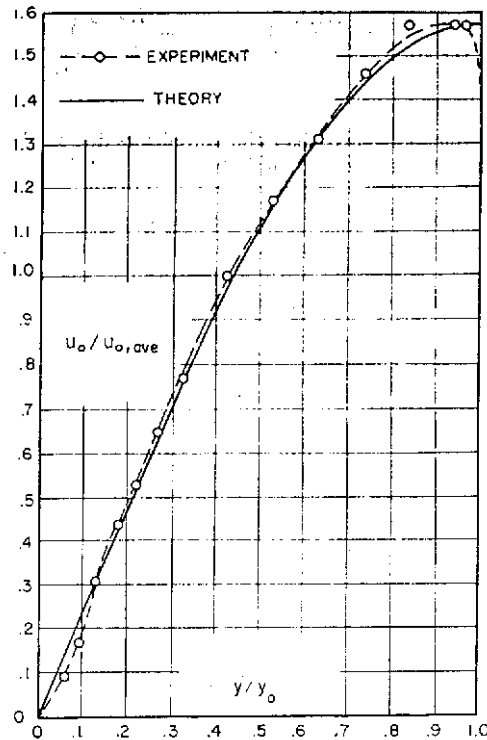


Fig. 7 The skewed velocity profile at the exit of the box-shaped outlet header. Equation (3a) compared with the test results. ($\delta U_o/U_{o,ave}$)_{ave} = 42 percent.

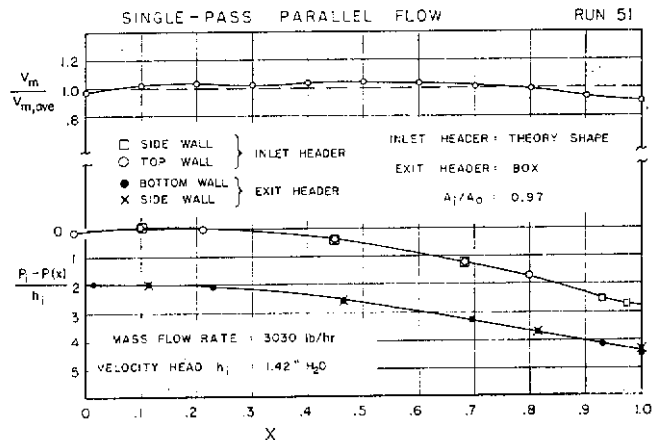


Fig. 8 Single-pass parallel flow header performance for the theory shaped inlet, Fig. 16. Note the one-dimensional behavior for the pressure.

$\sqrt{\Delta P_{matrix}/h_i}_{ave}$. The departure of $v_m/v_{m,ave}$ from unity is the velocity deviation from the average

$$\frac{\delta v_m}{v_{m,ave}} = \left| \frac{v_m}{v_{m,ave}} - 1 \right|$$

The average deviation of the velocity deviation is taken as the criterion of nonuniformity.

$$\text{Flow nonuniformity} = \left(\frac{\delta v_m}{v_{m,ave}} \right)_{ave}$$

The trapezoid rule is again used to form this average.

To estimate the penalty in heat transfer performance associated with a specified nonuniformity, it is recommended that the flow distribution be treated as suffering a step change (\pm) equal to the nonuniformity magnitude.

Clearly the flow nonuniformity factor is a characteristic of the

Table 3 Summary of test results

Header description	Test no.	Flow rate ω lbs/hr	Inlet vel head h _i H ₂ O	Pressure Drops				$\left(\frac{\delta v_m}{v_{m,ave}}\right)_{ave}$ %
				$\Delta P_{overall}$ h _i	ΔP_{matrix} h _i	ΔP_{outlet} h _i	$\Delta P_{t.headers}$ h _i	
Parallel flow	50	1997	0.615	4.54	2.29	2.34	2.31	3.4
Theory inlet and box exit.	51	3030	1.42	4.30	1.98	2.46	2.38	3.3
A _i /A ₀ = 0.97 ^c	52	3995	2.49	4.27	1.88	2.50	2.45	4.0
Parallel flow	22	2000	0.637	4.46	2.26	2.35	2.24	1.9
Theory inlet +0.020-in. spacer and box exit.	23	3015	1.45	4.30	2.06	2.52	2.28	1.8
A _i /A ₀ = 0.98	24	3970	2.53	4.26	1.90	2.56	2.40	2.2
Parallel flow	31	2010	0.632	4.00	2.29	2.34	1.77	8.3
Triangular inlet and box exit.	32	3010	1.425	3.96	2.04	2.56	1.98	11.0
A _i /A ₀ = 0.97	33	4015	2.55	3.81	1.86	2.52	2.01	11.4
Parallel flow								
Box inlet and box exit. A _i /A ₀ = 0.97	10	3000	1.42	3.50	1.97	2.75	1.59	21.0
Counterflow	53	1992	1.42	1.00	0.98	0.97	0.615	3.0
Box inlet and box exit.	54	3010	3.28	0.90	0.88	1.03	0.615	4.4
A _i /A ₀ = 0.636	55	4005	5.91	0.84	0.81	1.06	0.625	4.6
Counterflow	45	2005	1.162	1.58	1.28	1.23	0.80	4.5
Box inlet and box exit.	46	3015	2.64	1.40	1.08	1.23	0.82	6.2
A _i /A ₀ = 0.713	47	3985	4.68	1.35	1.02	1.30	0.83	6.4
Counterflow	38	2015	0.635	3.44	2.22	2.37	1.28	9.8
Box inlet and box exit.	39	2997	1.417	3.20	1.92	2.45	1.34	11.6
A _i /A ₀ = 0.97	40	3985	2.53	3.13	1.83	2.55	1.36	13.1
2-Pass parallel flow	48	2000	0.618	4.57 ^a	2.26 ^a	2.31 ^a	2.35 ^a	4.5 ^a
First pass: Theory inlet and box exit; A _i /A ₀ = 0.98				4.05 ^b	2.27 ^b	2.28 ^b	1.80 ^b	5.1 ^b
Second pass: Theory inlet and box exit. A _i /A ₀ = 0.99	49	3012	1.42	4.27 ^a	1.98 ^a	2.38 ^a	2.33 ^a	4.2 ^a
				3.78 ^b	1.92 ^b	2.36 ^b	1.88 ^b	5.2 ^b

^a First pass only.

^b Second pass only.

^c When A_i/A₀ < 1.0 $\frac{\Delta P_{t.headers}}{h_i} > \frac{\Delta P_{overall} - \Delta P_{matrix}}{h_i}$ by $\left(1 - \frac{h_0}{h_i}\right)$.

header and heat exchanger core system and not of the headers alone. If the core (matrix) pressure drop is large relative to the pressure changes in the headers, the influence of the headers on flow distribution will be minor. In the case of the test system, the pressure change in the matrix is approximately 2h_i (see Table 3). This is of the same order of magnitude as the pressure changes in the headers and, as a consequence, header performance has an important influence on the flow nonuniformity factor. It is believed that this situation is typical of gas turbine plant regenerators and intercoolers and many other gas flow heat exchanger systems.

Header Performance

The eight header configurations tested are listed in the first column in Table 3. The main test conditions and the header performance, as characterized by the loss ΔP_t/h_i and the flow nonuniformity (δv_m/v_{m,ave})_{ave}, are also tabulated. Representative graphs, Figs. 8-15, all for a nominal mass flow rate of 3000 lb/hr, provide the pressure profiles and the associate matrix flow distribution. For all these tests, ρ_i/ρ₀ can be treated as unity and z_i/y₀ as A_i/A₀ for comparison with the theory predictions.

The four single-pass parallel flow configuration tests will be considered first. The approach of the actual inlet header shape for runs 50, 51, and 52, the so-called "theory" inlet shape, to the geometry specified by equation (5) for z_i/y₀ = 1 and ρ_i/ρ₀ = 1, is reported in Fig. 16. Departures on the order of 3 percent of z_i may be noted. This lack of agreement undoubtedly contributes to the nonuniformity magnitude, averaging² about 3.6 percent.

The reduced flow area in the region of X ≥ 0.8 was considered to be the main factor contributing to flow nonuniformity (see Fig. 8); so for runs 22, 23, and 24 a 0.02-in-thick frame was used to produce the modified theory geometry reported in Fig. 17. The resulting nonuniformity was reduced to 2 percent. It is evident from Fig. 9, however, that for X > 0.9 the flow area is too great, so that P(X)_{inlet} does not drop off enough to match

² In the discussion where three test runs in a set are being evaluated arithmetic average values will be used.

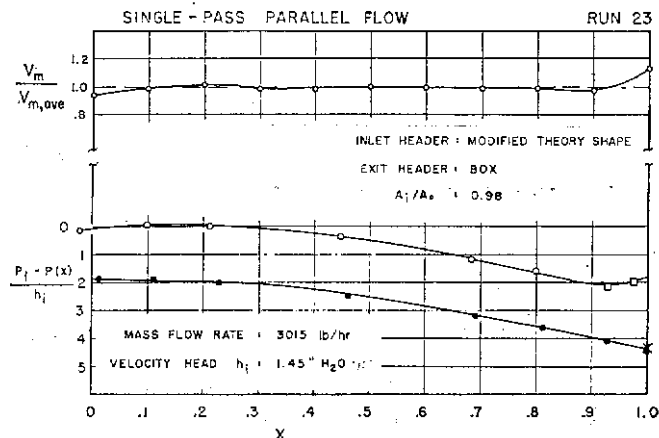


Fig. 9 Single-pass parallel flow header performance for a modified theory-shaped inlet, Fig. 17

the P(X)_{outlet} profile in this region. It is believed on the basis of this evidence that a closer approach to the theory geometry of equation (5) would indeed provide for better flow uniformity. However, for most exchanger applications a nonuniformity factor of 5 percent would be acceptable; and this can be achieved if the dimensions are maintained to ±2 percent of z_i and care is taken not to block off the smaller flow area region for X > 0.8.

The outlet header pressure profile for the theory and modified theory inlets, Figs. 8 and 9, very closely match the theory prediction of equation (2); ΔP_{outlet}/h_i is very close to the (π²/4) = 2.47 from equation (2). The header loss ΔP_t/h_i averages⁴ out to be 2.34 (runs 50, 51, 52, 22, 23, and 24, Table 3), which is 2 percent below the theory prediction of equation (14). This difference may be a boundary-layer effect as there is evidently a trend upward for ΔP_t/h_i with increasing flow rate. A flow rate of ω = 2000 lb/hr; run No. 50; corresponds to an inlet Reynolds number (based on the hydraulic diameter of A_i) of approximately 90,000.

⁴ In the discussion where three test runs in a set are being evaluated arithmetic average values will be used.

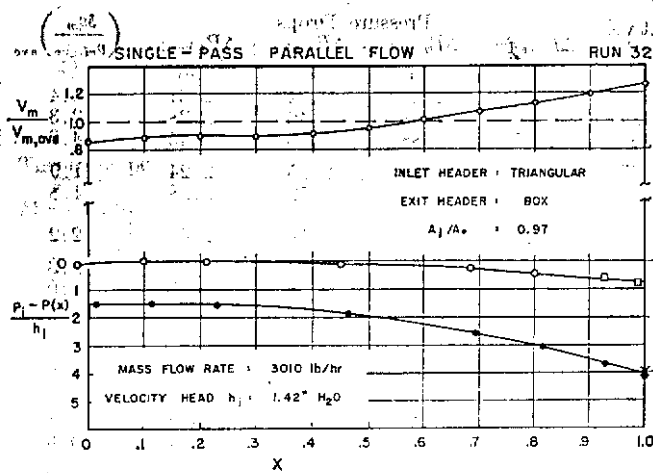


Fig. 10 Single-pass parallel flow header performance for a triangular-shaped inlet, Fig. 17

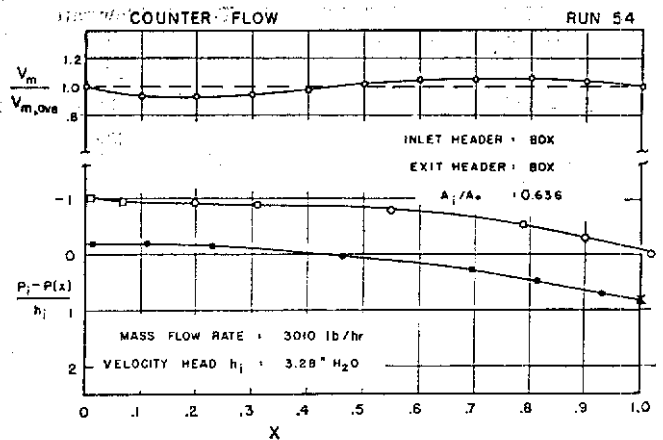


Fig. 12 Single-pass counterflow header performance for the theory-specified box headers

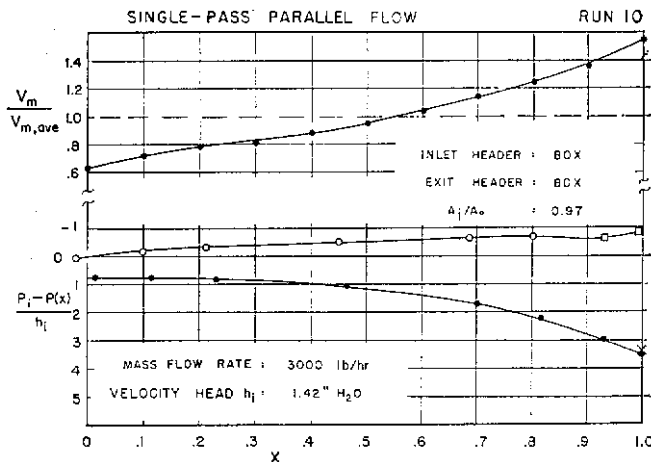


Fig. 11 Single-pass parallel flow header performance for a box-shaped inlet

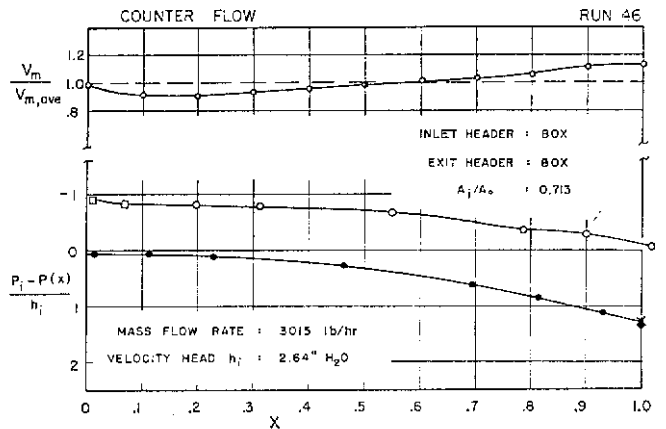


Fig. 13 Single-pass counterflow header performance for a 12 percent oversized inlet header

The triangular header shape is described in Fig. 17. Runs 31, 32, and 33, in Table 3, show that the nonuniformity averages 10 percent, which is substantially poorer than the performance of the theory shape of 2 to 4 percent. Fig. 10 shows the pressure profiles and the velocity distribution. Clearly, gross departures from the theory shapes result in serious flow nonuniformities and to accentuate this point, with a box header, run 10, and Fig. 11, a 21 percent nonuniformity results. Note, however, that the header loss, $\Delta P_i/h_i$, is reduced substantially from the theory value of 2.38. This point illustrates the fallacy of using the header loss as a criterion of design excellence. The lower loss is obtained only at the expense of the main function of the headers, to provide for close to uniform flow through the heat exchangers.

The three single-pass counterflow configurations listed in Table 3 will now be considered. The situation with $z_i/y_o = A_i/A_o = 0.636$ represents the theory shape when $\rho_o/\rho_i = 1$, equation (10). As can be seen from the entries for runs 53, 54, and 55, the flow nonuniformity factor averages at 4 percent which is considered to be quite acceptable, and the header head loss is $\Delta P_i/h_i = 0.62$ in comparison to the theory prediction of 0.60, equation (15). Fig. 12 shows the flow distribution and pressure profiles typical for this header. The pressure drop in the outlet header $\Delta P_{outlet}/h_i = 1.03$. From the theory equation (7)

$$\frac{\Delta P_{outlet}}{h_i} = \frac{\Delta P_{outlet}}{h_o} \frac{h_o}{h_i} = \frac{\pi^2}{4} \frac{4}{\pi^2} = 1.00$$

Thus, the agreement is quite excellent.

The second set of data, runs 45, 46, and 47, serves to demon-

strate the influence of departing from the theory specifications. The inlet header area is "oversized" by the ratio $(0.713/0.636)$, or 12 percent. As can be seen from Fig. 13 and the Table 3 entries, the flow nonuniformity is increased from 4 to 6 percent. The outlet header drop ($\Delta P_{outlet}/h_i$) is increased from 1.03 to 1.25, but when normalized relative to h_o becomes $(\Delta P_{outlet}/h_o) = (1/0.713)^2 \times 1.25 = 2.45$, which closely approximates the $\pi^2/4 = 2.47$ of the outlet header flow theory, equation (7). The header loss $(\Delta P_i/h_i) = 0.82$ when it is normalized relative to h_i , but as h_i is decreased by $(0.713/0.636)^2 - 1 = 26$ percent, ΔP_i is only increased by 5 percent.

The third set of data, runs 38, 39, and 40, illustrates the effect of a substantial oversizing by $(0.97/0.636) - 1 = 53$ percent. Now the average flow nonuniformity factor is significantly greater at 11.5 percent (Fig. 14). The outlet header drop $(\Delta P_{outlet}/h_o) = (\Delta P_{outlet}/h_i)(h_i/h_o) = (2.46)(1.063) = 2.62$, and this is within 6 percent of the theory prediction of $\pi^2/4 = 2.47$. Clearly, the theory boundary condition of $v_m = \text{const}$ is not closely approximated, but nevertheless the agreement is good. As a matter of interest, the parallel flow situation with the triangular inlet header, runs 31, 32, and 33, show about the same nonuniformity factor (10.2 percent average) and $\Delta P_{outlet}/h_o = 2.47$ is also the same. A comparison of Figs. 10 and 14 reveals a strong similarity in the character of the nonuniform v_m distribution. The header loss for the oversized inlet (counterflow), $(\Delta P_i/h_i) = 1.27$, but because of the lower h_i , in the ratio $(0.636/0.97)^2$, the ΔP_i is actually lower than for the theory shape by 14 percent. So again at the expense of the primary function of the header, namely, uniformity of flow distribution, a lower flow loss may be realized.

The last header configuration listed in Table 3, run 49, is the

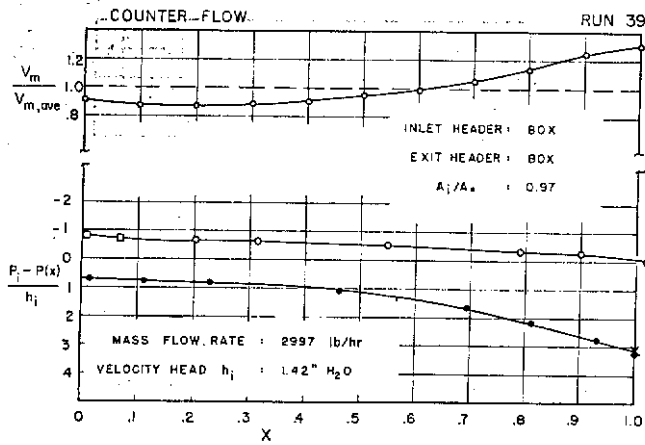


Fig. 14 Single-pass counterflow header performance for a 53 percent oversized inlet header

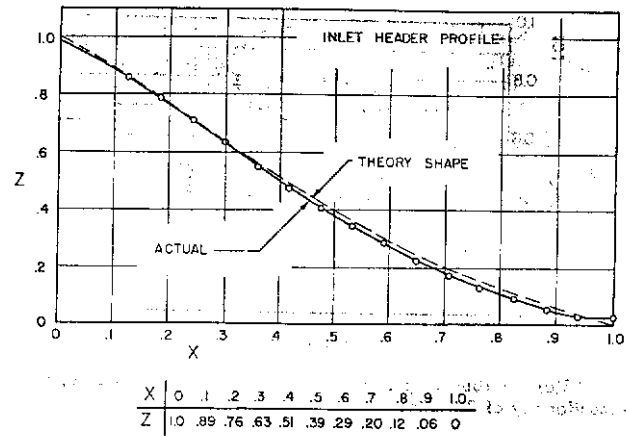


Fig. 16 Theory shape for the inlet header for the parallel flow configuration. Comparison of theory and laboratory model.

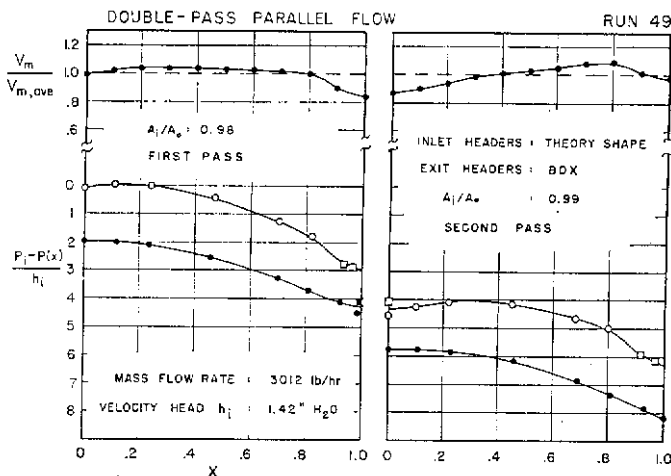


Fig. 15 Two-pass parallel flow header performance. See Fig. 7 for skewed velocity profile for the second pass inlet.

two-pass parallel flow configuration with single-pass theory-shaped inlets and box headers for each pass. Fig. 15 provides the pressure profiles and the flow distribution. In comparison to the comparable single-pass configuration, run 51, the first-pass behavior remains essentially unchanged, but the second-pass reveals a 23 percent lower loss with a one point increase in the nonuniformity from 4.2 to 5.2 percent. Before the tests, it was anticipated that the highly skewed velocity profile $u_0(y)$, Fig. 7, entering the second pass would tend to (a) increase the nonuniformity significantly and (b) increase the head loss for the second pass. The actual substantial reduction of head loss can be rationalized by the fact that of the $\Delta P_1/h_1 = \pi^2/4 = 2.47$ predicted by the theory for the first pass, 0.645 (26 percent) is assigned to the exit header, equation (18), and this is really a bookkeeping loss of kinetic energy associated with the convention of using the bulk average velocity to calculate the flow stream kinetic energy. The heat exchanger designer will welcome this fortunate circumstance. It also suggests that for single-pass configurations, substantial nonuniformity in the inlet header velocity profile can be tolerated.

Inlet Velocity Profile Tests

The test results for the two-pass parallel flow configuration pointed out the need to investigate the influence of nonuniformity in the inlet flow. A velocity profile generator described in [3] was used to generate the $u_i(z)$ profiles shown in Figs. 18(b, c, d). Fig. 18(a) shows the normal duct profile, without the installation of the profile generator, which is typical of conditions for the tests reported in Table 3. Fig. 18(b) shows a more uni-

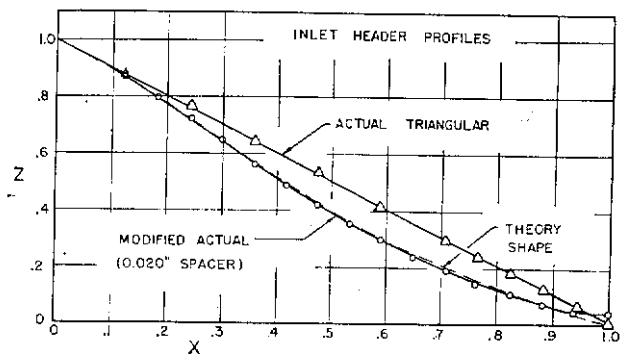


Fig. 17 Laboratory models for the modified theory-shaped and triangular-shaped inlet headers for the parallel flow configuration

form profile obtained by appropriate adjustments of the profile generator. Fig. 18(c) shows the laboratory approximation of a linear profile with a "favorable" skew⁵ and Fig. 18(d) a linear profile with an "unfavorable" skew. Nine sets of tests are presented in [3], covering a range of u_i nonuniformities⁶ from 3.7 percent for the profile, Fig. 18(b), to as high as 42 percent for the favorable skew profile in Fig. 7. These results are too extensive to cover in detail here. Only the main conclusions will be presented.

1 The more *uniform profile*, Fig. 18(b), did show a small improvement over the turbulent profile, Fig. 18(a), with respect to matrix flow uniformity.

2 The *favorable skew profile*, Fig. 18(c), resulted in a smaller header loss, with no penalty in matrix flow nonuniformity for the counterflow configuration; while for the parallel flow configuration the header loss is decreased slightly, but the matrix flow nonuniformity is increased moderately.

3 The *unfavorable skew profile*, Fig. 18(d), resulted in virtually the same header loss, with a significant increase in the matrix flow nonuniformity for the counterflow configuration; while for the parallel flow configuration the header loss is increased slightly and the matrix flow nonuniformity is increased significantly.

4 For a favorable skew and a very strong nonuniformity, as characterized by Fig. 7, for the inlet to the second-pass of the two-pass parallel flow configuration, the header loss is reduced significantly but the matrix flow nonuniformity is increased moderately.

⁵ The terms favorable and unfavorable derive from qualitative arguments that the nonuniformity of $u_i(0, z)$ involves a smaller penalty in terms of matrix flow nonuniformity and pressure drop if $du_i(0, z)/dz$ is positive in the main flow region.

⁶ The nonuniformity of the inlet velocity profile is defined as $(\delta u_i / u_{i,ave})_{ave}$ as obtained by a 10 ordinate analysis of the test profile.

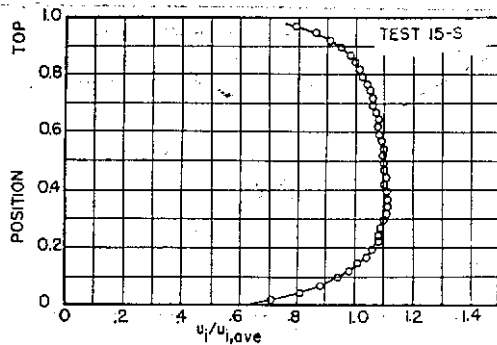


Fig. 18(a) Turbulent profile characteristic of developed duct flow. Nonuniformity of 8 percent.

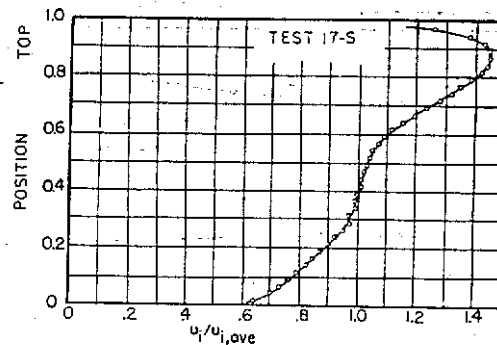


Fig. 18(c) Generator produced approximation to a linear, favorable skew profile. Nonuniformity of 18.4 percent.

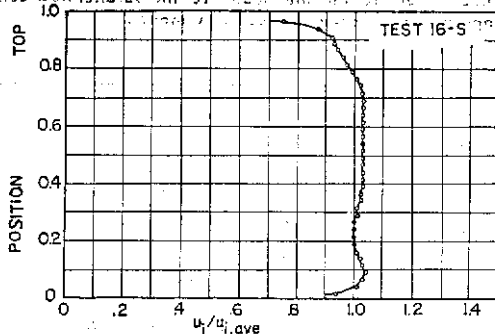


Fig. 18(b) Generator produced approximation to uniform flow profile. Nonuniformity of 3.7 percent.

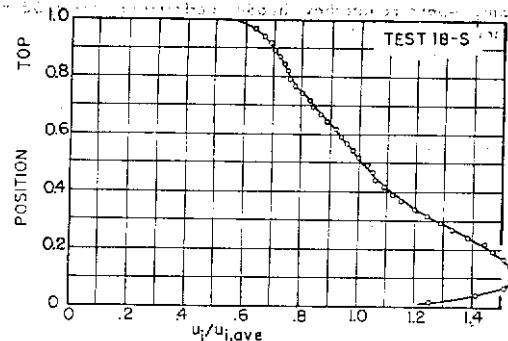


Fig. 18(d) Generator produced approximation to a linear, unfavorable skew profile. Nonuniformity of 23.8 percent.

Fig. 18 Experimental inlet velocity profiles $u_i(z)$. See Fig. 7 for the sine shape, favorably skewed profile with a nonuniformity of 42 percent.

5 If a matrix flow nonuniformity of 5 percent is acceptable, an inlet profile nonuniformity of up to 20 percent can be tolerated with either a favorable or unfavorable skew. A favorable skew profile, however, is to be preferred if the option is available.

6 It does not appear to be practical to reduce by design the matrix flow nonuniformity below 3.5 percent because it would then be necessary to insure a very uniform inlet velocity profile and this is not considered to be feasible except in a laboratory situation.

Free Discharge Header

The free discharge header configuration in Fig. 2 was not investigated experimentally in the present program. However, the theory results are presented, equation (16), and Loeffler and Perlmutter [4, 6] have demonstrated good experimental verification of the theory.

Application to Design

It is evident from the test results that equations (2)-(6c) for the parallel flow and equations (7)-(11c) for the counter flow configuration can be used as a basis for design. The test results of the theory-shaped headers support both the idealizations of the analysis and the resulting design equations. Also the analysis of flow stream mechanical energy losses chargeable individually to the inlet and exit headers, equations (17) and (18), are supported by the test results. Moreover, the "off-theory" header tests illustrate the type and magnitude of the penalty to be paid in terms of nonuniformity of flow over the heat exchanger surfaces.

The purposes of this section are to illustrate the header sizing procedure by a specific example and to discuss other design considerations.

In [8] an example is presented for the design of a cross-flow regenerator core for a 5000 hp gas turbine plant. The following

relevant information is extracted for the purpose of designing the headers for the compressor airflow which is heated on passing through the regenerator.

Regenerator effectiveness	$\epsilon = 75$ percent
Air-side core pressure drop	$\Delta P/P_i = 0.42$ percent
Airflow densities	$\rho_i = 0.438$ pcf
	$\rho_0 = 0.300$ pcf
	$\rho_i/\rho_0 = 1.46$
Matrix frontal area	$A_m = 3 \times 7.5 = 22.5$ sq ft
Airflow rate	$\omega = 193,000$ lb/hr = 53.7 lb/sec
Inlet air pressure	$P_i = 132$ psia

For the single-pass *parallel flow* header design, it will be specified that the inlet header initial velocity $u_i = 100$ fps and that the exit header will be sized so as to make $h_0 = h_i$. Under these conditions

$$h_0 = h_i = \rho_i \frac{u_i^2}{2g_c} = 68.0 \text{ #/sq ft} = 13.1 \text{ }^{\circ}\text{H}_2\text{O} = 0.472 \text{ #/sq in.}$$

$$A_i = \frac{\omega}{u_i \rho_i} = 1.225 \text{ sq ft}$$

$$u_{0,ave} = \sqrt{2g_c h_0 / \rho_0} = 121 \text{ fps}$$

$$A_0 = \frac{\omega}{\rho_0 u_{0,ave}} = 1.48 \text{ sq ft}$$

$$A_i/A_0 = 0.828$$

For the single-pass *counterflow* header design, it is only necessary to specify u_i , taken as before as 100 fps. One cannot impose an arbitrary relationship between h_0 and h_i as this condition is fixed by the theory equation (11c). In applying the theory, the ratio z_i/y_0 will be taken as equivalent to A_i/A_0 . The implication is that the z -section of the headers need not be rectangular

as specified in the mathematical models. It is believed that this is a valid approximation for smoothly contoured header walls.

Parallel Flow Header

From equation (6c) with $h_0 = h_i$

$$\left(\frac{\rho_i}{\rho_0}\right)\left(\frac{A_i}{A_0}\right)^2 = 1 \text{ and } \frac{A_i}{A_0} = \sqrt{\frac{1}{1.46}} = 0.828$$

This checks the previously derived result.

Introducing equation (6c) into equation (5) yields

$$Z = \frac{(1-X)}{\left(\frac{\rho_i}{\rho_0}\right)^{1/2} \left[\frac{\pi^2}{4} X^2 + \frac{h_i}{h_0} \right]^{1/2}}$$

With $h_i/h_0 = 1$ the following tabulation for the header shape results:

X	0	0.25	0.50	0.75	1.00
$Z = A_i/A_0$	0.828	0.577	0.324	0.134	0
A sq ft	1.225	0.855	0.480	0.198	0
x for $L = 7.5$ ft	0	1.875	3.75	5.62	7.5

The header loss may be evaluated from equation (14)

$$\frac{\Delta P_i}{h_i} = 1.47 \frac{h_0}{h_i} + 1 = 2.47$$

$$\frac{\Delta P_i}{P_i} = \frac{2.47 \times 0.472}{132} = 0.883 \text{ percent}$$

From equation (18) the exit header loss is $0.645 h_0 = 0.645 h_i$, 26 percent of the total. From equation (17b), the inlet header loss is $1.822 h_i$ or 74 percent of the total.

Counterflow Header

From equation (11c)

$$\frac{h_0}{h_i} = \frac{4}{\pi^2} = 0.405$$

With u_i specified as 100 fps, $h_i = 68 \text{ \#/sq ft}$, so

$$h_0 = 27.5 \text{ \#/sq ft}$$

$$\frac{u_0}{u_i} = \sqrt{\frac{h_0}{h_i}} \sqrt{\frac{\rho_i}{\rho_0}} = \sqrt{0.405} \sqrt{1.46} = 0.770$$

$$u_0 = 77 \text{ fps}$$

$$\frac{\rho_0 u_0^2}{2g_c} = h_0 = \frac{0.30 \times 77^2}{64.4} = 27.6 \text{ \#/sq ft (check)}$$

From equation (10)

$$Z = \text{const} = \frac{A}{A_0} = \frac{A_i}{A_0} = 0.636 \sqrt{\frac{\rho_0}{\rho_i}} = 0.526$$

For $A_i = 1.225 \text{ sq ft}$ (with $u_i = 100 \text{ fps}$)
 $A_0 = 2.33 \text{ sq ft}$

From equation (15)

$$\frac{\Delta P_i}{h_i} = 0.595$$

$$\frac{\Delta P_i}{P_i} = \frac{0.595 \times 0.472}{132} = 0.213 \text{ percent}$$

From equation (18) the exit header loss is $0.645 h_0 = 0.645 \times 0.405 h_i = 0.261 h_i$, or 44 percent of the total. From equation (17c) the inlet header loss is $0.333 h_i$, or 56 percent of the total.

The parallel flow and counterflow designs are compared in the following tabulation.

	Parallel flow	Counterflow
Inlet velocity u_i , fps	100	100
Exit velocity u_0 , avg, fps	121	77
Inlet area A_i , sq ft	1.225	1.225
Exit area A_0 , sq ft	1.48	2.33
Inlet header area $A(x)$	See tabulation	Constant at A_i
Exit header area $A(x)$	Constant at A_0	Constant at A_0
Header losses $\frac{\Delta P_i}{h_i}$	2.47	0.595
$\frac{\Delta P_i}{P_i}$, percent	0.883	0.213
Fraction for inlet header, percent	74	56
Fraction for outlet header, percent	26	44

As a point of interest, it is noted that for the parallel flow design the header loss of 0.88 percent exceeds the calculated heat exchanger surface pressure drop of 0.42 percent [8, p. 256], by more than twofold. It is also clear that the counterflow design, though somewhat more bulky (see the A_0 comparison) is very much to be preferred if the machinery arrangement will allow this configuration.

Because the core pressure drop is small relative to the pressure changes in the headers, in the ratio of $0.42/0.88 = 0.48$, the header performance can be expected to have a greater influence on the nonuniformity factor than for the tests, for example, where the ratio was on the order of 0.8. Consequently, the designs summarized in the foregoing can be expected to have larger flow nonuniformities of the order of 5 percent, in comparison to the test results of 2 to 4 percent.

Moreover, for the parallel flow design, the inlet header dimensions must adhere fairly close to the theory, about ± 2 percent of A_i , as in Figs. 16 and 17. For the exit header no such precision is required. Both box headers for the counterflow configuration are less sensitive to off-specification dimensions in terms of the nonuniformity factor.

Both designs can tolerate fairly nonuniform inlet velocity conditions (up to 20 percent) without too much of a penalty in flow nonuniformity.

It appears that the single-pass counterflow header theory could be used to design a sharp return bend for a relatively small loss of about $0.60 h_i$ by using a low resistance matrix such as HEXCEL (1 or 2-in. flow length) to function as turning vanes.

The test performance of the two-pass parallel flow configuration indicates that the single-pass theory provides quite a good basis for design as indicated by the test flow nonuniformity factors of only about 5 percent. This is a result of the lack of sensitivity of header performance (second-pass inlet) to a favorable skewed inlet velocity profile.

Summary and Conclusions

The previous text deals with the design of single-pass header systems of the parallel flow and counterflow types. Both the theory and test results are presented. Based on this information the following conclusions result:

1 An adequate design basis for single-pass parallel flow and counterflow header configurations now exists; that is, optimum geometries can be specified, expected losses can be estimated, and reasonably good flow distribution uniformity (± 5 percent) over the heat exchanger surfaces can be anticipated.

2 Parallel flow headers will have losses of the order of four times that of counterflow configurations.

3 The header performance is relatively insensitive to inlet velocity distribution.

4 Close adherence to the theoretical shape is necessary for the inlet header for the parallel flow design.

5 A two-pass parallel flow header can be designed using single-pass theory largely because of item 3.

6 The influence of flow nonuniformity on heat exchanger performance deterioration can be calculated in specific instances.

using an extension of the heat exchanger design theory presented in [8]; such calculations are provided in [1]. Generally the penalty is greater for high design effectiveness, for C_{min}/C_{max} approaching unity, and for situations where a "high" for one fluid stream is opposite a "low" for the other fluid stream.

The free discharge configuration described in Fig. 2 may be of special interest to air-conditioning heat exchanger designers. Header losses are intermediate to the counterflow and parallel flow configurations.

References

- 1 Wilson, D. G., "A Method of Design for Heat-Exchanger Inlet Headers," ASME Paper No. 66-WA/HT-41.
- 2 London, A. L., Klopfert, G., and Wolf, S., "Oblique Flow Headers for Heat Exchangers—The Ideal Geometries and the Evaluation of Losses," TR No. 63, Department of Mechanical Engineering, Stanford University, Stanford, Calif., Aug. 1966.
- 3 Klopfert, G., "Oblique Flow Headers for Heat Exchangers—The Influence of Inlet Velocity Profiles," TR No. 65, Department of Mechanical Engineering, Stanford University, Stanford, Calif., July 1967.
- 4 Perlmutter, M., "Inlet and Exit Header Shapes for Uniform Flow Through a Resistance Parallel to the Main Stream," *Journal of Basic Engineering*, TRANS. ASME, Series D, Vol. 83, No. 3, Sept. 1961, pp. 361-370.
- 5 Heyda, J. F., "An Analytical Study of a Balanced Reverse Folded Flow," General Electric Company Report XDC 60-1-153, reprinted by Department of Commerce, Jan. 1960. See also the discussion of [4] by Heyda, J. F., and Fulton, C. D.
- 6 Loeffler, A. L., and Perlmutter, M., "Turbulent Flow Through Porous Resistances Slightly Inclined to the Flow Direction," NACA TN 4221, 1958.
- 7 Wolf, S., "Flow Losses for Heat Exchangers With Oblique Flow Headers," TR No. 60, Department of Mechanical Engineering, Stanford University, Stanford, Calif., June 1964.
- 8 Kays, W. M., and London, A. L., *Compact Heat Exchangers*, 2nd ed., McGraw-Hill, New York.

APPENDIX

Analysis of Oblique Flow Models

The analysis presented here was first developed by Heyda [5] for the counterflow configuration. This method of analysis was then used by Wolf [7] for the parallel flow configuration. The repetition in this Appendix is for the purpose of summarizing the two solutions and the methodology, using a uniform nomenclature. Additionally, the oblique flow inlet free discharge configuration is analyzed.

The mathematical models analyzed are described in Fig. 19. The outlet header analysis will apply to both the parallel and counterflow configurations and will be given first. Then the inlet header for the parallel flow configuration will be analyzed, followed by the inlet header for the counterflow configuration. Finally, the inlet header of the free discharge configuration is analyzed.

The outlet shape is specified as rectangular⁷

$$Y(X) = 1$$

and the pressure profile is derived for a uniform velocity leaving the matrix, assuming pressure a function of X only, but allowing the streamline velocity to be a function of x and y . Then the inlet header shape is selected to provide a $P(X)$ which matches the exit header profile, thereby maintaining a constant ΔP_{matrix} and a uniform flow distribution ($v_m = \text{const}$) through the matrix; see Fig. 4.

Outlet Header. When the Navier-Stokes' equations are expressed for steady, constant density, inviscid flow, the y -gradient of the pressure may be expressed

$$\frac{\partial P}{\partial y} = \frac{\rho_0}{g_c} \left[u \frac{\partial v}{\partial x} + v \frac{\partial u}{\partial y} \right] \quad (23)$$

The box header has the smallest pressure drop for a given exit area.

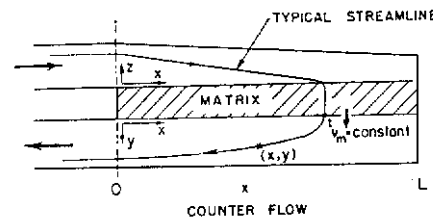
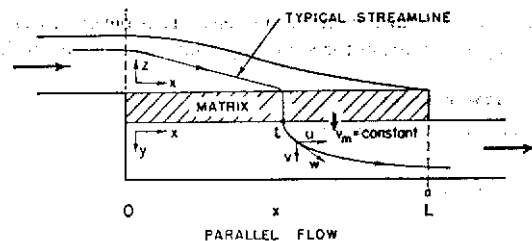


Fig. 19(a)

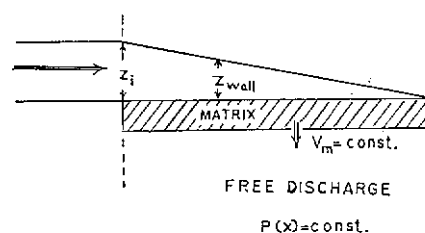
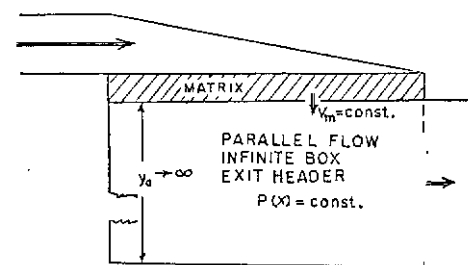


Fig. 19(b)

Fig. 19 Mathematical models for the three single-pass header configurations

But as P is specified to be a function of x only, the y -pressure gradient is zero, and this condition imposed on equation (23) leads to

$$v = \text{const} (= v_m) \quad (24)$$

The Navier-Stokes' equations may also be integrated along the streamline originating at point t in Fig. 19 to yield the Bernoulli equation for incompressible flow

$$P(x) + \frac{\rho_0}{2g_c} (u^2 + v^2) = P(t) + \frac{\rho_0}{2g_c} v_m^2$$

In light of equation (24) this reduces to

$$P(t) - P(x) = \rho_0 \frac{u^2}{2g_c} \quad (25)$$

From the continuity principle applied for constant density to the stream tube bounded by the streamlines originating at t and $(t + dt)$ (using the coordinates in Fig. 19),

$$-(u dy) = v_m dt \quad (26)$$

Using this result for u and substituting into equation (25) yields

$$-dy = v_m \sqrt{\rho_0/2g_c} \frac{dt}{\sqrt{P(t) - P(x)}} \quad (27)$$

This equation may be integrated to yield the wall contour $y_{wall}(x)$ by integrating between the limits

$$\begin{aligned} \text{for } t = 0, y &= y_{wall}(x) \\ \text{for } t = x, y &= 0 \end{aligned}$$

Thus

$$y_{wall}(x) = \int_{y_{wall}(x)}^0 (-)dy = \int_0^{t=x} v_m \sqrt{\rho_0/2g_c} \frac{dt}{\sqrt{P(t) - P(x)}} \quad (28)$$

This is a Volterra improper integral equation which has been solved by Heyda [5] for some simple header shapes, $y_{wall}(x)$. For the box header shape considered here, y_{wall} is constant and the solution yields⁸

$$P(0) - P(x) = \frac{\pi^2}{4} \rho_0 \frac{u_{0,ave}^2}{2g_c} \left(\frac{x}{L}\right)^2 = \frac{\pi^2}{4} h_0 X^2 \quad (29)$$

If the origin for x is taken at the outlet header section farthest away from the exit, this result will apply for the outlet box header for both the parallel and counterflow configurations, Fig. 19.

With the pressure profile known, one can determine the exit velocity u_0 as a function of $y_{x=L}$. From the Bernoulli equation (25)

$$P(t) - P(L) = \rho_0 \frac{u_0^2}{2g_c} \quad (30)$$

But

$$\begin{aligned} P(t) - P(L) &= \{[P(0) - P(L)] - [P(0) - P(t)]\} \\ &= \frac{\pi^2}{4} h_0 - \frac{\pi^2}{4} h_0 \left(\frac{t}{L}\right)^2 \\ &= \frac{\pi^2}{4} h_0 \left[1 - \left(\frac{t}{L}\right)^2\right] \end{aligned} \quad (31)$$

from equation (29). Equating (30) and (31)

$$\frac{u_0}{u_{0,ave}} = \frac{\pi}{2} \sqrt{1 - \left(\frac{t}{L}\right)^2} \quad (32)$$

Introducing u_0 from the continuity equation (26), separating variables and integrating

$$-\int_{y_0}^{y_{x=L}} dy_{x=L} = \frac{2}{\pi} \frac{y_0}{L} \int_0^t \frac{dt}{\sqrt{1 - \left(\frac{t}{L}\right)^2}}$$

The result is

$$\frac{y_{x=L}}{y_0} = \left[1 - \frac{2}{\pi} \sin^{-1} \frac{t}{L}\right] \quad (33)$$

Solving for (t/L) and substituting in equation (32) yields the desired exit velocity u_0 as a function of $y_{x=L}$

$$\frac{u_0}{u_{0,ave}} = \frac{\pi}{2} \cos \frac{\pi}{2} \left(1 - \frac{y}{y_0}\right) = \frac{\pi}{2} \sin \left(\frac{\pi}{2} \frac{y}{y_0}\right) \quad (34)$$

This equation may be used to relate the actual exit kinetic energy rate to the nominal value calculated from the bulk average velocity. The result is

⁸ $v_m L = u_{0,ave} y_0$ from continuity is used here.

$$\begin{aligned} \frac{(KE_0/\omega)_{actual}}{(h_0/\rho_0)} &= \frac{(u_0^3)_{ave}}{(u_{0,ave})^3} = \frac{\pi^2}{16} \left[\frac{\sin 3\theta}{3} + \frac{3 \sin \theta}{3} \right]_{\theta=0}^{\pi/2} \\ &= \frac{\pi^2}{6} = 1.645 \end{aligned} \quad (35)$$

$$\text{where } \theta = \frac{\pi}{2} \left(1 - \frac{y}{y_0}\right)$$

Equations (29), (34), and (35) are the important results for the exit box header, used for both the single-pass parallel flow and counterflow configurations. The idealizations and specifications involved are as follows:

- 1 Constant density flow, $\rho = \rho_0$.
- 2 The flow through the matrix is uniform, $v_m = \text{const.}$
- 3 Pressure is a function of x only.
- 4 Zero flow stream mechanical energy dissipation (inviscid flow).

Inlet Header, Parallel Flow. For this analysis it is idealized that pressure and velocity are essentially functions of x only and that the density is constant. Then the Bernoulli equation for the streamline in Fig. 19 is

$$P_i - P(x) = \frac{\rho_i}{2g_c} (u^2 - u_i^2) \quad (36)$$

For constant density flow the continuity principle provides the following relations for a uniform input velocity, $u_i = \text{const.}$ and uniform flow distribution through the core, $v_m = \text{const.}$

$$\left. \begin{aligned} u_i z_i &= u z_{wall} + v_m x = v_m L \\ u z_{wall} &= v_m (L - x) \\ u_i z_i \rho_i &= u_{0,ave} y_0 \rho_0 \end{aligned} \right\} \quad (37)$$

The pressure profile of equation (36) is required to match that of the exit header, equation (29). So

$$P_i - P(x) = \frac{\pi^2}{4} h_0 \left(\frac{x}{L}\right)^2 \quad (38)$$

Combining equations (38), (37), and (36) to eliminate P and u provides the desired inlet header shape, z_{wall} , as a function of x .

$$\frac{\rho_i}{\rho_0} \left(\frac{\pi^2}{4} X^2\right) = \left[\frac{(1 - X)^2}{Z^2} - \left(\frac{y_0}{z_i}\right)^2\right]$$

or

$$Z^2 = \frac{(1 - X)^2}{\left(\frac{\rho_i}{\rho_0}\right) \left(\frac{\pi^2}{4}\right) X^2 + \left(\frac{y_0}{z_i}\right)^2} \quad (39)$$

Note that

$$\frac{h_0}{h_i} = \frac{\rho_i}{\rho_0} \left(\frac{z_i}{y_0}\right)^2$$

Substitution of the header shape back into the continuity equation (37) will yield inlet header velocity as a function of x

$$\frac{u}{u_i} = \sqrt{\frac{\rho_i}{\rho_0} \left(\frac{z_i}{y_0}\right)^2 \frac{\pi^2}{4} X^2 + 1} \quad (40)$$

This relation may be used to establish the kinetic energy per unit mass flow rate leaving the inlet header and passing into the core.⁹

⁹ Note that v_m in equation (41a) is the matrix velocity based on A_m at the inlet face of the matrix, in contrast to the v_m pictured in Fig. 19 which is the matrix velocity at the outlet face.

$$\frac{KE}{\omega} = \frac{1}{v_m \rho_i L} \int_0^L \frac{u^2}{2g_0} \rho_i v_m dx \quad (41a)$$

The result is

$$\frac{(KE/\omega)}{(h_i/\rho_i)} = 1 + \frac{\pi^2}{12} \left(\frac{z_i}{y_0}\right)^2 \left(\frac{\rho_i}{\rho_0}\right) = 1 + 0.822 \left(\frac{z_i}{y_0}\right)^2 \left(\frac{\rho_i}{\rho_0}\right) \quad (41b)$$

Note the difference relative to equation (35) where the kinetic energy term involves a $(u^2)_{ave}$ instead of a $(u^2)_{ave}$ as in the foregoing.

The important results for the inlet header in the single-pass parallel flow configuration are equations (38), (39), (40), and (41b). The idealizations and specifications involved are as follows:

- 1 Constant density flow, $\rho = \rho_i = \text{const.}$
- 2 Both pressure and velocity are essentially functions of x only.
- 3 Zero flow stream mechanical energy dissipation.
- 4 The flow through the matrix is uniform, $v_m = \text{const.}$
- 5 The entering flow is uniform, $u_i = \text{const.}$
- 6 The pressure profile matches that of the exit box header.

Inlet Header, Counterflow. For this analysis, as for the parallel flow inlet header, it is idealized that pressure and velocity are essentially functions of x only and that the density is constant. Then the Bernoulli equation for the streamline indicated in Fig. 19 is the same as equation (36). Also from the continuity principle, the (37) set of equations apply. However, in order to satisfy a pressure match with the exit header, equation (29) requires a shift in coordinates because of the counterflow configuration. The pressure profile then becomes

$$P(x) - P_i = \frac{\pi^2}{4} h_0 [1 - (1 - X)^2] \quad (42)$$

That is, the inlet header now has to function as a diffuser with a flow deceleration in contrast to the parallel flow situation where the flow is accelerated. Combining the Bernoulli equation (36) with continuity, equation (37), and the pressure match conditions, equation (42), to eliminate P and u , provides the desired inlet shape z_{wall} as a function of x .

$$Z^2 = \frac{(1 - X)^2}{\left(\frac{y_0}{z_i}\right)^2 - \left(\frac{\rho_i}{\rho_0}\right) \left(\frac{\pi^2}{4}\right) [1 - (1 - X)^2]} \quad (43)$$

To avoid imaginary values for Z it is necessary that the denominator of equation (43) be positive or

$$\left(\frac{y_0}{z_i}\right)^2 > \left(\frac{\rho_i}{\rho_0}\right) \left(\frac{\pi^2}{4}\right) [1 - (1 - X)^2]$$

The maximum value of the right-hand side is $(\rho_i/\rho_0)(\pi^2/4)$ for $X = 1$. So

$$\left(\frac{y_0}{z_i}\right)_{\max} = \frac{2}{\pi} \sqrt{\rho_0/\rho_i} = 0.637 \sqrt{\rho_0/\rho_i}$$

Following Heyda [5], this value for z_i/y_0 will be accepted as the "economic size," as smaller magnitudes would have a higher h_i and higher losses of kinetic energy when the flow enters the matrix. When this optimum (z_i/y_0) magnitude is introduced into equation (43) the optimum header shape becomes

$$Z^2 = \frac{4}{\pi^2} \frac{\rho_0}{\rho_i} = \text{const} \quad (44)$$

That is, the optimum inlet shape is also a box header.

Substitution of this header shape back into the continuity equation (37) yields the inlet header velocity as a function of x

$$\frac{u}{u_i} = 1 - X \quad (45)$$

Following the procedure used in establishing equation (41b), the kinetic energy per unit flow rate leaving the inlet header and passing into the core is

$$\frac{KE_i/\omega}{(h_i/\rho_i)} = \frac{(u^2)_{ave}}{u_i^2} = \frac{1}{3} \quad (46)$$

The important results for the inlet header in the single-pass counterflow configuration are equations (42), (44), (45), and (46). The idealizations and specifications involved are the same as for the inlet header for the parallel flow configuration and are listed after equation (41b).

Oblique Flow Inlet, Free Discharge. A technically interesting variation of the parallel flow configuration is pictured in Fig. 19. If the outlet header is made very deep, ($y_0 \rightarrow \infty$), the outlet pressure profile becomes uniform. This is also the situation for the free discharge configuration shown in Fig. 19. This header configuration is quite commonly found in air-conditioning heat exchangers where the free discharge of the conditioned air is directed into the room. It would also be the situation on the hot gas side of a gas turbine regenerator discharging straight up an exhaust stack. Under these circumstances equation (39) for the inlet header shape reduces to

$$\frac{z_{wall}}{z_i} = (1 - X) \quad (47)$$

i.e., a triangular shape. This solution is the same as presented by Loeffler and Perlmutter [6].

This result can also be derived directly from the Bernoulli equation (36), and the continuity equation (37), and the pressure profile matching condition. From equation (36) and the pressure profile matching condition, $P(x) = \text{const}$,

$$u = u_i = \text{const}$$

Then from the second of equations (37)

$$\frac{z_{wall}}{z_i} = \frac{v_m L (1 - X)}{u z_i} = \frac{v_m L (1 - X)}{u_i z_i}$$

Introducing $u_i z_i = v_m L$ from the first of equations (37) yields equation (47).

From equation (41a), the defining equation for KE/ω

$$\frac{(KE/\omega)}{(h_i/\rho_i)} = 1 \quad (48)$$

This also comes directly from equation (41b) for $y_0 \rightarrow \infty$.

DISCUSSION

A. A. Kudirka¹⁰

The authors are to be congratulated for presenting a useful method supported by experimental results for designing oblique flow headers. However, a designer would be also very much interested in the limits of applicability of the design equations presented in the article.

In the authors' tests, performed to demonstrate the validity of their design method, the pressure change in the matrix was equal to about two velocity heads of the inlet header, i.e., $2h_i$. It has been the writer's experience that one-dimensional analysis is no longer useful in guiding header design when the pressure change in the matrix is equal to about one-half h_i . Similarly, the usefulness of the design equations must be also limited to headers with certain z_i/L ratios.

¹⁰ Development Engineer, General Electric Company, San Jose, Calif. Assoc. Mem. ASME.

Of course, it may be specified that the design equations are applicable to "reasonable" or "characteristic" geometries and pressure changes, but, quantitative limits would be more helpful to the designer.

It may be also noted that the header designs discussed produce a pressure gradient in the longitudinal x -direction (see Figs. 4(a) and 4(b)) in the matrix. This pressure gradient will cause longitudinal flow to occur in the matrix unless this matrix is of special design. Since such flow may be detrimental to performance in some designs, it may be avoided by designing inlet and outlet headers which theoretically produce no longitudinal pressure gradient.

For the parallel flow configuration, for example, the inlet header would have the shape shown in Fig. 4(c), and the shape of the outlet header for $v_m = \text{const}$ (nomenclature of the article is used) would be $Y = (x/L)^2$. This shape is arrived at by combining the one-dimensional continuity and momentum relationships for the outlet header.

R. L. Wong¹¹

AiResearch has available an operational computer program to handle the general problem of oblique flow headers and core flow distribution. The computations in general are based on the theories presented in this paper. The following comments are offered related to the analysis:

1 We are in agreement with the experimental work reported. The inlet header pressure profiles for headers of the type similar to the "parallel flow theory inlet shape" are very sensitive to header shape and core flow distribution—particularly near the closed header end. This sensitivity is due to the high velocity heads required to obtain the desired drop in static pressure at this end.

2 Compressibility increases the dimensionless inlet header static pressure change, $\Delta P/h_i$, in the "box inlet header." This increase is due to the recovery of the inlet total pressure which is greater than $(P_i + h_i)$. This difference becomes significant at Mach numbers greater than 0.3. For air at an inlet Mach number of 0.6857 with uniform header and core flow,

$$\frac{\Delta P}{h_i} = 1.000 \text{ for incompressible flow}$$

$$\frac{\Delta P}{h_i} = 1.121 \text{ for compressible flow}$$

3 In the "triangular inlet header," there is no pressure recovery and hence also no static pressure change. Consequently, the flow in this header (for uniform core flow) reflects no compressibility effects.

4 In the "parallel flow theory inlet shape," the compressibility effects result in a decreasing fluid density from the inlet end to the closed end. Hence one would expect the static pressure change to be increased.

5 In the "box outlet headers," the dimensionless static pressure change is decreased by the effects of compressibility. At an outlet Mach number (based on uniform outlet flow) of 0.5678 with uniform core flow

$$\frac{\Delta P}{h_o} = 2.47 \text{ for incompressible flow}$$

$$\frac{\Delta P}{h_o} = 2.28 \text{ for compressible flow}$$

The compressibility effects are reflected in two factors, both of which contribute to the decreased static pressure change:

¹¹ Preliminary Design Engineering Department, Heat Transfer Group, AiResearch Manufacturing Company, Los Angeles, Calif.

(a) The average fluid density increases from the open header and to the closed end.

(b) The outlet flow profile is more uniform in compressible flow.

For incompressible flow:

$$\frac{\text{maximum } (\rho u_o)}{(\rho u_o)_{\text{ave}}} = 1.571$$

$$\frac{(\rho u_o^3)_{\text{ave}}}{(\rho_{\text{ave}} u_o^3)_{\text{ave}}} = 1.645$$

for compressible flow:

$$\frac{\text{maximum } (\rho u_o)}{(\rho u_o)_{\text{ave}}} = 1.428$$

$$\frac{(\rho u_o^3)_{\text{ave}}}{(\rho_{\text{ave}} u_o^3)_{\text{ave}}} = 1.382$$

The more uniform outlet flow profile is due to the increasing fluid density from

$$\frac{\rho}{\rho_{\text{ave}}} = 0.935 \text{ at } \frac{y}{y_o} = 0.0$$

to

$$\frac{\rho}{\rho_{\text{ave}}} = 1.045 \text{ at } \frac{y}{y_o} = 1.0$$

This outlet density profile follows from two assumptions:

- (a) The static pressure is one dimensional.
- (b) There is no heat transfer between streamlines.

The following additional comments are offered on this paper:

1 In the next to the last paragraph of the section "Application to Design" we would like some elaboration as to how the Hexcel functions as turning vanes.

2 In the "Summary and Conclusions," the second conclusion applies only to the headers and not to the entire heat exchanger package.

Also, if one is willing to accept the resulting flow maldistribution (say because of a high core pressure drop) the parallel flow and counterflow configurations could have similar losses.

Authors' Closure

Mr. Kudirka's points regarding limits of applicability of the design equations are well taken. Tentatively it is suggested that

$$\frac{\Delta P_{\text{matrix}}}{h_i} > \frac{1}{2}$$

$$\frac{A_i}{A_m} \left(\text{or } \frac{z_i}{L} \right) < \frac{1}{3}$$

The lower limit on ΔP_{matrix} is Mr. Kudirka's recommendation, and the area ratio limit derives from the authors' intuition that the one-dimensional treatment of the pressure variation, $P(x)$ only, is not adequate if the header is too deep in the z -direction.

Certainly a pressure gradient dP/dx will tend to result in some longitudinal flow if transverse partitions are not built into the heat exchanger core. The relative flow, longitudinal-to-transverse, will vary directly as the relative pressure gradients and inversely as the relative flow impedances. For the screen matrices used in the tests the relative longitudinal flow is estimated as less than 2 percent.

Mr. Kudirka's suggestion that a triangular inlet header and a parabolic outlet header would provide a parallel flow configuration with a zero longitudinal pressure gradient can only be correct for a very deep outlet header ($y_o \rightarrow \infty$) approaching the free discharge configuration of Fig. 4(c).

Mr. Wong's comments are appreciated for two reasons. First, it is satisfying to know that Mr. Wong's organization finds the theory useful as a design tool. Normally "proof of the pudding" is not so rapidly forthcoming. Secondly, the effects of departures from the constant density idealization (noncompressed flow) in each of the headers are important in aircraft applications where high subsonic Mach number duct flow is common.

The authors' prefer *noncompressed flow* instead of *incompressible flow*, as the preferred term suggests that the density is approximately constant by virtue of the small pressure and temperature changes within a header, rather than the implication of the second term that the density *can't change*, as for an incompressible liquid flow.

In Mr. Wong's first group of numbered comments it is important to note that comment 2 applies to a diffusing or decelerating flow inlet header, such as for the counterflow configuration of Fig. 4(b), while comment 4 applies to an accelerating flow inlet header.

In comment 5 relating to the accelerating flow in the outlet box headers, the density decreases in the flow direction. This is in agreement with Mr. Wong's statement of an "increase from the open end to the closed end" as this is counter to the flow direction.

In summary of Mr. Wong's first group of numbered comments, items 2 to 5, the general conclusion regarding Mach number or compressibility effects is that the noncompressed flow theory under-predicts the magnitude of the pressure change in both accelerating and decelerating header. This conclusion could be anticipated from one-dimensional diffuser and nozzle theory. It is not clear what the proper geometries are for these high Mach Number headers. It is hoped that Mr. Wong will clarify this point by preparation of a paper in the near future.

With respect to Mr. Wong's second group of comments the following remarks are offered:

1 In view of Mr. Kudirka's experience that if $\Delta P_{\text{matrix}}/h_i < 1/2$ the theory is not applicable, the authors do not recommend their sharp return bend design suggestion, unless verifying tests are forthcoming.

2 This comment is well taken and in the final analysis it is indeed the header heat exchanger system overall pressure drop that is important.

Authors' correction: The abscissa on the counterflow header performance curves, Figs. 12, 13, and 14, should be changed to $(1-X)$ to conform to the definition of X in Fig. 4(b).